PORTABLE X/ -RAY SURVEY METER BASED ON THE INTERNET OF THINGS NETWORK FOR MEASURING THE ENVIRONMENTAL RADIATION DISTRIBUTION

by

Simin XIAO*, Xinglong LI, Yang LIU, Zhiping LUO, Hongchao PANG, Jianhua WU, and Xiaopeng HUANG

China Institute of Atomic Energy, Beijing, China

Scientific paper
https://doi.org/10.2298/NTRP2401029X

Real-time detection of X/gamma radiation dose rates holds particular significance in nuclear science research. In this study, we developed a portable X/gamma-ray survey meter for large-scale distributed real-time monitoring of ambient dose equivalent rates in the surrounding environment. This innovative device uses a silicon photomultiplier coupled with a CsI(Tl) scintillator and can connect to an Internet of Things network. Additionally, it facilitates a wide spectrum of dose rate measurements by modifying the frequency of a pulse-frequency modulation-type DC-DC power supply mode. The energy response of the survey meter, which is improved through Geant4 simulations and a multi-comparator design, ranges from 48 keV to 1.3 MeV, encompassing various common protection level applications. It effectively measures gamma radiation dose rates ranging between 0.1 Svh^{-1} and 100 $mSvh^{-1}$ for ^{60}Co. Temperature compensation of the detector was achieved through a series of experiments. The meter exhibits a deviation of –25 % to +25 % at temperatures between –40 °C and +40 °C.

Key words: CsI(Tl) scintillator, silicon photomultiplier, X/ -ray survey meter, blue tooth, Internet of Things

INTRODUCTION

Nuclear radiation detection is a pivotal technology within nuclear science and its practical applications span nuclear power operation, safety protocols, homeland security, and beyond [1, 2]. Among these applications, real-time detection of X/ radiation dose rates holds particular significance as a crucial research avenue. In the context of emergency radiation monitoring, real-time dose rates serve as a rapid and intuitive indicator of abnormal radioactive levels that can promptly trigger alarms if the radioactivity surpasses defined thresholds. Therefore, real-time dose rates emerge as the paramount parameter in X/ radiation detection [3, 4].

In the context of emergency radiation monitoring, real-time dose rates serve as a rapid and intuitive indicator of abnormal radioactivity levels. They promptly trigger alarms if the radioactivity surpasses defined thresholds. Therefore, real-time dose rates emerge as the paramount parameter in X/ radiation detection [5].

Radiation protection technicians traditionally relied on handheld radiation survey meters or vehicle-mounted detectors for radiation monitoring during initial environmental investigations. However, this approach requires significant manpower and cannot capture measurement data from multiple time points.

The prevalence of portable X/ survey meters in radiation monitoring stems from their lightweight design and user-friendly nature. Leveraging the Internet of Things (IoT) system, a network of interconnected wireless radiation measurement devices can be established. This network integrates data from various portable radiation detectors to execute radiation detection and localization within the designated area. This capability facilitates advanced search and monitoring functionalities across expansive coverage areas, even in emergency scenarios. Presently, numerous countries have embraced IoT-based radiation monitoring systems [6].

In this paper, we present a novel approach to environmental radiation monitoring across expansive regions-a distributed small survey meter that combines mobile phone technology with an IoT network. Each survey meter is assigned a unique identifier, facilitat-

* Corresponding author, e-mail: 15701607305@163.com

ing network access and ensuring accurate positioning and status information. Collaboratively, multiple survey meters and mobile phones form a smart radiation monitoring system, proficient in large-scale surveillance. This comprehensive system serves a diverse array of functions, including radiation measurement, positioning, and manual alarm activation. Such capabilities transcend the limitations of conventional manual radiological surveys, mitigating personnel workload while enhancing the efficiency of environmental monitoring.

Typical X/ survey meters are constrained by pulse width and electronic limitations, typically offering a range between 0.1 μSvh^{-1} and 1 $mSvh^{-1}$. For measuring a wide range of X/ dose rates spanning from 0.1 μSvh^{-1} to 100 $mSvh^{-1}$, a common design approach involves employing a dual probe detector. This setup incorporates a small area probe tailored for high dose rate measurements (ranging from 1 $mSvh^{-1}$ to 100 $mSvh^{-1}$) alongside a larger area probe dedicated to low dose rate measurements (falling within the range of 0.1 μSvh^{-1} to 1 $mSvh^{-1}$). Alternatively, this can be achieved using a hybrid measurement mode of pulse and current. The entire circuit needs to be matched with a dual preamplifier, main amplifier, and comparator to obtain pulse (or current) signals. This type of circuit system takes up a lot of space, consumes high power, and has high costs. The paper adopts a pulse-frequency modulation PFM-type DC-DC boost circuit to design and implement a wide-range radiation measurement circuit based on a power switch module. The size of the analog circuit is 20 mm × 23 mm, and power consumption is less than 30 μA (environmental background). The developed CsI(Tl) survey meter is proficient in measuring ambient dose equivalent of H*(10) with exceptional sensitivity for X/ rays, spanning an energy range of 48 keV to 1300 keV. It effectively covers a dose rate range of 0.1 μSvh^{-1}-100 $mSvh^{-1}$.

MATERIALS AND METHOD

The comprehensive structure is depicted in fig. 1. It incorporates a CsI(Tl) detector and a PFM-type DC-DC boost circuit for X/ ray dose rate detection. Additionally, a mobile application is utilized to furnish location data, exhibit radiation measurement values, trigger over-threshold alarms, and facilitate Internet data uploads. Complementing this, a web application is used to display the device distribution, radiation measurements, and historical data for multiple devices on a map.

Detector design

The detector has compact dimensions of 75 mm × 35 mm × 15 mm, thereby ensuring convenient portability, and it can be operated continuously for 24 hours in an external environment. The analog control section of the detector encompasses a DC-DC boost circuit, silicon photomultiplier (SiPM), CsI(Tl), and a comparator module. The CsI(Tl) volume measures 5 mm × 5 mm × 5 mm, enveloped by a 0.3 mm-thick TiO_2 reflective layer on its five surfaces to heighten reflection.

The electronic component comprises both analog and digital circuits. Within the realm of analog circuits, an amplifier-less design was formulated. In instances where the SiPM registers a scintillation light pulse, the signal pulse amplitude from the SiPM attains ample magnitude, obviating the need for an amplifier and enabling direct connection to the comparator. This circuit configuration offers the advantage of streamlined complexity by minimizing the quantity of affixed electronic elements, consequently curbing detector power consumption.

The SiPM interfaces with a four-channel comparator, allocating three channels for energy response

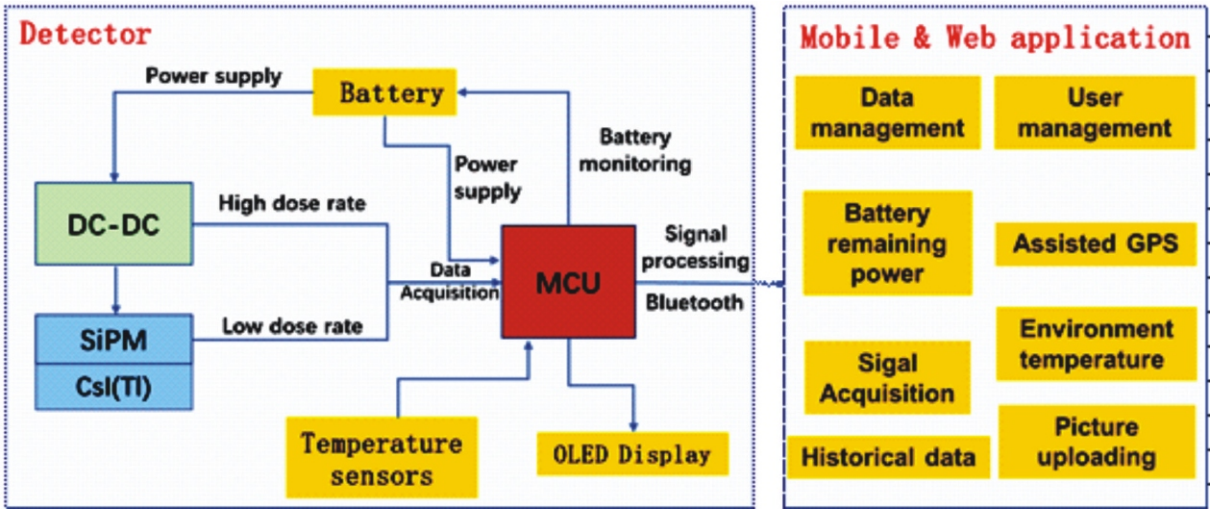

Figure 1. Structural diagram of the detection system

calibration and low-dose rate measurements, while reserving one channel for high-dose rate measurements.

Owing to the increased sensitivity of the CsI(Tl) scintillator to low-energy X-rays and the subsequent stabilization in energy response at higher energy levels, we opted for a tungsten compensator combined with a segmented energy measurement method to ensure consistent detection performance across a wide spectrum of X/ -ray energies. This approach involves employing three high-speed comparators to establish distinct voltage thresholds (V1-V3), effectively dividing the flashing pulse energy into three bands: E1-E3. The trigger threshold of the three-way comparator spans from low to high, covering energies ranging from 48 keV to 1.3 MeV. Whenever the pulse voltage surpasses a specific threshold, the corresponding comparator generates a high-level signal. Notably, the lowest threshold is set slightly above the circuit's noise level to ensure comprehensive triggering of all flashing pulse signals.

Scintillation light pulses (flashes) entail a pulse rise and decay time. The decay time of a scintillator signifies the interval following which the light pulse intensity regresses to 1/e of its peak value. For X/ rays, CsI(Tl) boasts an average decay time of approximately 1 s. This characteristic may result in pulse pileup during applications with a high count rate.

Therefore, we employed a pulse-frequency modulation (PFM)-type DC-DC power supply to cover the high dose rate range (1 $mSvh^{-1}$-100 $mSvh^{-1}$).

The PFM control strategy hinges upon a rectangular pulse train to ascertain the output voltage of the regulator. Different from adjusting the duty cycle of a fixed-frequency pulse train to establish the output voltage (PWM), PFM manipulates the frequency of a fixed-duty cycle pulse train. During PFM operation, the output power is directly proportionate to the average frequency of the pulse train, and the converter operates when the output voltage drops below the set output voltage as measured by the feedback control loop. Subsequently, the switching frequency of the converter is elevated progressively until the output voltage converges upon the designated set output voltage. This frequency modulation of DC-DC converter switching is harnessed for measuring the high dose rate ranging from 1 $mSvh^{-1}$ to 100 $mSvh^{-1}$.

As illustrated in fig. 2. Sig1 encompasses pulse counting for low dose rates, whereas Sig2 governs pulse counting for high dose rates. The U1 is a PFM-type DC-DC power converter responsible for boosting the power supply voltage VIN and providing it to the SiPM as a bias voltage. The U2 and U3 are comparators. The pulse signals generated by SiPM and CsI (Tl) are AC coupled to U3 through C2, used for measuring low-dose rates(background to 1 $mSvh^{-1}$).

When using the detector at a high dose rate range (1 $mSvh^{-1}$ to 100 $mSvh^{-1}$), varying dose rates result in different photocurrents i_1 generated by the SiPM. While the load resistance remains unchanged, an increase in iamer i_1 causes Voltage V_1 to rise. Consequently, the voltage of the SW pin decreases, prompting the power inductor switch to implement voltage adjustments, thereby ensuring voltage stability. In such instances, U1 adjusts the SW pin to alter the switch's frequency, thereby maintaining a steady output voltage V_1. When the U1 switch is turned on, an AC voltage signal V_2 is generated at the VIN pin, and V_2 is AC coupled to U2 through C1 to measure the switching frequency of the U1. The switching frequency of U1 is directly proportional to both the photocurrent i_1 generated by the SiPM and the X/ -ray dose rate, thus enabling measurements within the high dose rate range.

The method for measuring high radiation dose rates using a PFM-type DC-DC boost circuit is essentially achieved by measuring the current generated in SiPM. The analog circuits only include a single CsI(Tl) probe, DC-DC boost circuit, and multiple comparators, which occupie a small space and have low power consumption.

Temperature compensation is accomplished by incorporating thermistors into the analog circuitry. Rt1 and Rt2 are linear thermistors that form a voltage di-

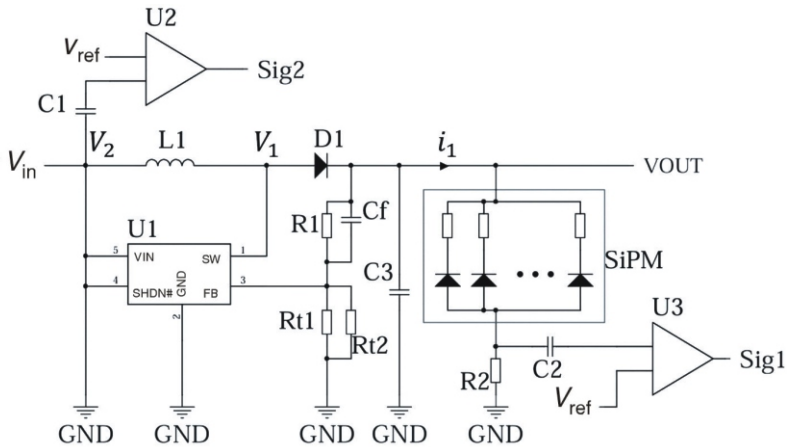

Figure 2. Analog circuits

vider circuit with R1 and R2. This configuration divides the reference voltage output by U1, generating a reference voltage that fluctuates in response to temperature variations. This variable voltage is then fed into the feedback input (FB) pin of U1, where U1 adjusts the output voltage VOUT based on the input voltage at the FB pin. Consequently, changes in the resistance of Rt1 and Rt2 due to temperature alterations lead to fluctuations in VOUT, effectively minimizing variations in SiPM gain.

The operational quantity for area monitoring, as suggested by the ICRP, is the ambient dose equivalent $H^*(10)$. This study employs a straightforward counting technique, which involves the utilization of the counting rate-dose rate conversion coefficient. This coefficient requires the detector to exhibit a uniform energy response across the designated energy range to yield the corresponding dose rate of $H^*(10)$.

$$H^*(10) \quad N_L(E_i)R_L(E_i), \quad \text{background} \sim 1 \text{ mSvh}^{-1}$$
$$H^*(10) \quad N_H(E_i)R_H(E_i), \quad 1 \text{ mSvh}^{-1} \sim 1 \text{ mSvh}^{-1}$$

where $R_L(E_i)$ and $R_H(E_i)$ are the counting-to-ambient-dose-equivalent conversion coefficients at low and high dose rates, respectively, cps/(Svh^{-1}), $N_L(E_i)$ is the pulse count generated by the SiPM, and $N_H(E_I)$ is the pulse count originating from the DC-DC power supply.

The analog circuit board is designed as a separate circuit board and is welded to the main board through stamp holes. The circuit board is sized 23 mm × 20 mm × 1.6 mm, has an operating voltage of 5V, and draws a current of approximately 26 A in an environmental background (measured by a KEITHLEY 2611B SYSTEM Source Meter).

Mobile and web application

An iOS and Android mobile application (app) was developed, fig. 3. By establishing Bluetooth connectivity with the detector, the app can retrieve and display the dose rate, cumulative dose, detector power, and detector number on its homepage. The mobile application transmits the data to a web server, which processes and stores the data within a database, and subsequently renders the processed data accessible over the Internet for users. In scenarios where an extensive array of survey meters is deployed across a specific region, the web app permits the monitoring of pollution distribution in the said area. This empowers administrators to swiftly comprehend the situation and take prompt actions in case of emergencies.

PERFORMANCE

Effect of temperature on the detection system

The relationship between the gain of SiPM and temperature, as well as the operating voltage, follows a linear pattern. Consequently, the gain of SiPM can be stabilized across varying temperatures by adjusting the operating voltage. With each 1° C increase in the temperature, the influence on SiPM gain corresponds to a voltage reduction of 0.033 V. Thus, to uphold consistent SiPM gain, a simultaneous 0.033 V voltage increase is necessitated for each 1 °C temperature rise.

Our approach focuses on minimizing the impact of the temperature by adjusting the reverse voltage. This adjustment is accomplished by varying the resistance value of the thermistor according to the temperature. An experimental assessment with a ^{241}Am source was conducted to test the CsI(Tl) scintillator and SiPM across a range of temperatures. In the experiments, a 30 000 Bq ^{241}Am source was affixed 2 cm above the CsI(Tl) scintillator and SiPM. The CsI(Tl) scintillator captured the 59 keV emission from the ^{241}Am -ray source, and the X-ray signals were amplified before being collected by the CAEN-N957 multichannel analyzer. The performance of the CsI(Tl) and SiPM was quantified across the temperature range of –40 °C to 40 °C and subjected to linear fitting. Figure 4 indicates

Figure 3. Graphical User Interface (GUI) of the survey meter and main interface on the application (a), GUI of the map page on the web application (b)

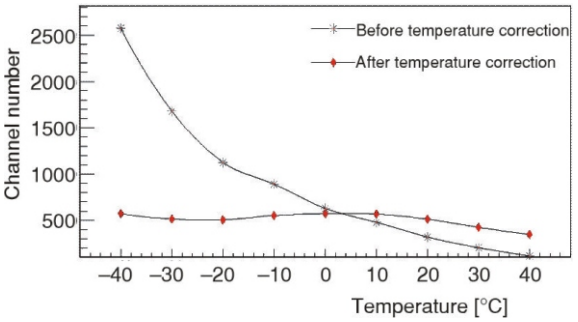

Figure 4. Temperature response of the detector before and after temperature calibration

that the temperature sensitivity of the detector is within –25 % to +25 % deviation in the range of –40 °C to +40 °C after temperature correction.

The X/ -ray energy response

A compensator combined with a segmented energy measurement method is employed to achieve a uniform energy response. The Geant4 simulation toolkit was used to determine the compensatory material and thickness. The simulated scintillator crystal, CsI(Tl), featured a Tl concentration of 0.15 % with a density of 4.51 gcm^{-3} [7]. The refractive index of CsI(Tl) was 1.79 across the emission wavelength range of 350-700 nm. The optical photon absorption length was set at 50 cm. The absolute light yield was fixed at 54000 photons per MeV. The decay time constants were assigned the values of 630 ns and 1000 ns for the fast and slow components, respectively, with the fast component yield ratio set at 0.6 [8]. Optical simulation at the surfaces was conducted using the UNIFIED model of GEANT4. The CsI(Tl) and TiO_2 were modeled as ground front-painted and dielectric-dielectric surfaces, whereas the CsI(Tl) and SiPM surfaces were modeled as polished and dielectric-metal surfaces, respectively [9]. Guided by these simulation outcomes, compensators composed of tungsten plates, 1 mm in thickness and with a 1.5 mm diameter punching area, were selected.

Characterization of the energy dependence response employed -rays from ^{137}Cs and ^{60}Co sources, and X-ray beams conforming to the specifications of China National Standard GB/T 4835.1-2012. The CsI(Tl) scintillator measurements were conducted using a reference X-ray beam with energies ranging from 48 keV to 211 keV, alongside ^{137}Cs at 662 keV and ^{60}Co at 1250 keV. The X-ray beams emanated from a tunable X-ray machine and ranged from 55 kV to 210 kV. The detector was sequentially irradiated each time at an ambient dose rate $H^*(10)$ of 100 μSvh^{-1}, employing the various photon sources. The simulated and experimental results of using a tungsten compensator for energy response compensation, as depicted in fig. 5, exhibit a discrepancy in the detector counting rates of less than 10 % for the same energy levels between simulation and experimentation.

The tungsten compensator is only useful for compensating the energy response of low-energy X-rays. In this study, a segmented energy measurement method was used to compensate for the energy

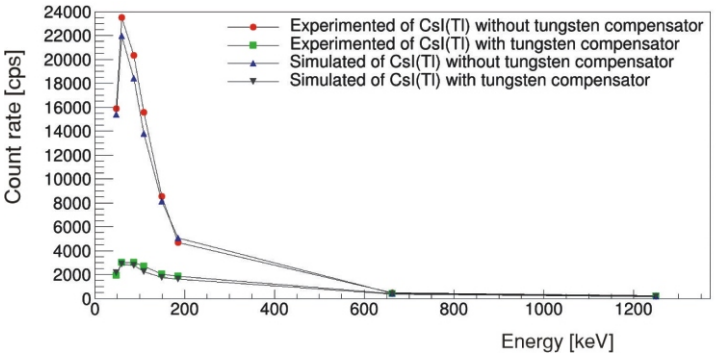

Figure 5. Comparison between Geant4 simulations and experimental results

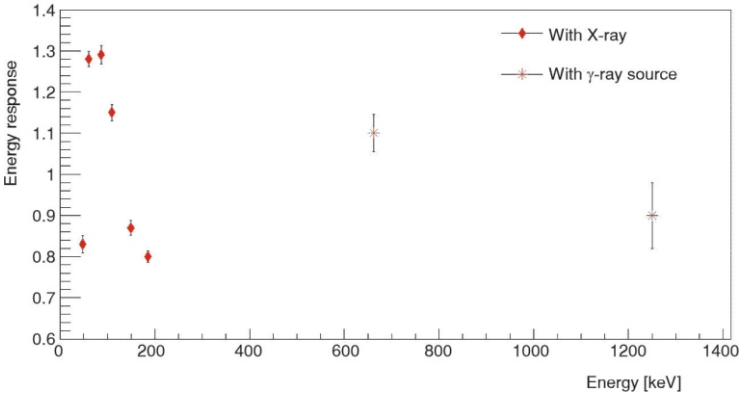

Figure 6. Energy response of the survey meter to H^* (10)

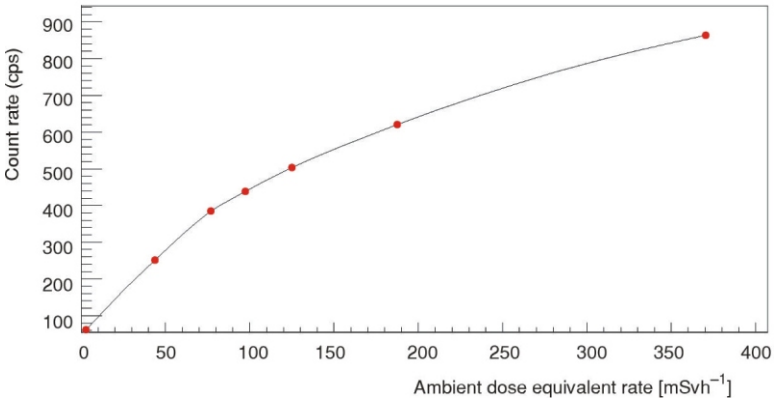

Figure 7. Linear response of the survey meter to ambient dose equivalent rate for ^{60}Co in the high-dose-rate measurement mode

response from 48 keV to 1.3 MeV. Figure 6 shows the acquired energy responses to H^* (10), encompassing energies ranging from 48 keV to 200 keV in the X-ray mode, photons at 1250 keV from the ^{60}Co source with an activity of 66.96 GBq for the -ray mode, and photons at 662 keV from the ^{137}Cs source ranging from 0.418 to 80.3 GBq for the -ray mode. The energy responses to H^* (10) in both X-ray and -ray modes deviate within the range of –20 % to +30 %.

Wide-range radiation field experiment

Drawing upon the outlined fundamental methods and principles, the detector was segmented into two ranges, each corresponding to distinct system parameters, and enabling dose rate measurements spanning from 0.1 Svh^{-1} to 100 mSvh^{-1}. To validate this design, various radiation experiments were conducted across diverse dose rates within the ^{60}Co and ^{137}Cs radiation fields. Notably, the γ radiation dose rate ranged from 0.1 Svh^{-1} to 7 mSvh^{-1} for ^{60}Co; 0.1 Svh^{-1} to 22 mSvh^{-1} for ^{137}Cs, in the context of the 615 calibration laboratory of the China Institute of Atomic Energy (CIAE) (standard field); and 1 mSvh^{-1} to 370 mSvh^{-1} for the ^{60}Co irradiation center at the CIAE (non-standard field). We determined dose rates at the test site employing compact CsI(Tl) and silicon detectors calibrated within the standard field. The counting rate of the survey meter was measured at a dose rate ranging between 3 and 370 mSvh^{-1}. The results are depicted in fig. 7, which reveals a deviation from linearity in the dose curve beyond 80 mSvh^{-1}. Higher dose rates (>100 mSvh^{-1}) require segmented calibration, *i. e*., the application of distinct calibration coefficients to different dose rate ranges. However, in this paper, we only applied calibration to the 100 mSvh^{-1} range.

As displayed in fig. 8, the departure of the response of the survey meter from the dose rate linearity falls within the range of 20 %, spanning from 1 Svh^{-1} to 100 mSvh^{-1}. Each error bar represents the corresponding standard deviation.

CONCLUSIONS

This paper describes the construction of an X/ -ray survey meter designed to measure ambient dose equivalent H^* (10) during emergency radiation monitoring or routine environental assessments. The detector employs a 5 mm × 5 mm × 5 mm CsI(Tl) scintillator coupled with a 3 mm × 3 mm SiPM, which enables the measurement of X/ -ray energy within the range of 48 keV to 1.3 MeV. The dose rate was tested using ^{60}Co radiation ranging from 0.1 μSvh^{-1} to 100 mSvh^{-1}.

The dose rate measurement in the detector range 1-100 mSvh^{-1} was increased by switching the frequency of a PFM-type DC-DC boost circuit. Compensation for the photon energy response of the CsI(Tl) scintillator was achieved using a multichannel comparator. Additionally, Monte Carlo simulations using the Geant4 toolkit were conducted to assess various compensator materials, thicknesses, and punching areas. Furthermore, the temperature-gain curve of SiPM was employed to correct the output temperature of the detection system.

Connectivity was established between the survey meter and mobile phones through Bluetooth, while an Internet connection was facilitated via Wi-Fi, thereby enabling a wider range of applications. In contrast to prevalent handheld radiation monitors, this device offers distinct advantages, including multipoint and multi-user capabilities, long-range monitoring, and real-time supervision. The survey meter is suitable for routine inspections in nuclear power plants, isotope production facilities, and warehouses in which radioactive sources are stored. Moreover, it is useful for emergency measurements during nuclear incidents and early warning monitoring for large-scale anti-nuclear terrorism activities.

While using Bluetooth communication, the distance between the phone and the detector during the use of this device cannot exceed 100 m. Although Bluetooth communication is efficient in terms of power consumption and offers good security, the data transmission speed is relatively slow, with a maximum speed of only tens of Mbps. For certain high-dose radi-

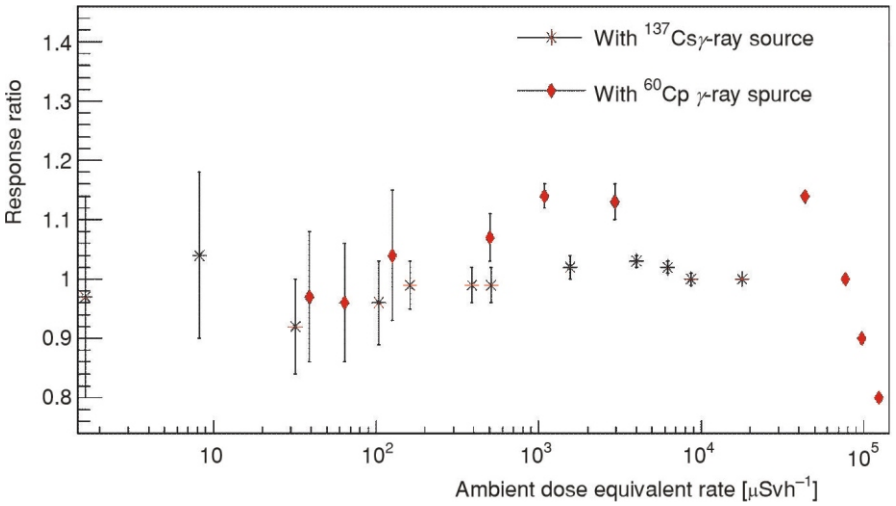

Figure 8. Dose rate linearity of the survey meter

ation areas that remain inaccessible to humans, LoRa or NB-IoT (Narrowband Internet of Things) modules offer a viable solution. These modules are suitable due to their capacity to facilitate communication over distances exceeding 5 km in urban settings and their ability to penetrate building structures.

Future efforts will focus on refining the system in the following areas: Minimizing system power consumption and extending the operational duration, and expanding the dose rate measurement range of the system to attain a dose rate of 1 Svh^{-1}.

ORCID ID

Simin XIAO: 0000-0002-3253-1223
Xinglong LI: 0000-0002-3262-9885
Jianhua WU: 0009-0009-8253-9256

REFERENCES

[1] Marques, L. A., *et al*., State-of-the Art Mobile Radiation Detection Systems for Different Scenarios, *Sensors, 21* (2021), 4, 1051
[2] Li., X. X., *et al*., New Experimental Measurement of Ernat (n, γ) Cross Sections Between 1 and 100 eV, *Physical Review C, 104* (2021), 5, pp. 054302
[3] Manzano., L. G., *et al*., An IoT LoRaWAN Network for Environmental Radiation Monitoring, *IEEE Trans. Instrum. Meas., 70* (2021), 6008512, pp. 1-12
[4] Li., X. X., *et al.*, Experimental Determination of the Neutron Resonance Peak of Er162 at 67.8 eV, *Physical Review C, 106* (2021), 6, 065804
[5] Tziortzioti., C., *et al*., IoT Sensors in Sea Water Environment: Ahoy! Experiences from a Short Summer Trial, *Electronic Notes in Theoretical Computer Science, 343* (2019), 5, pp. 117-130
[6] Quang, V. T., Viet, H. D., An Internet of Radiation Sensor System (IoRSS) to Detect Radioactive Sources Out of Regulatory Control, *Sci. Rep, 12* (2022), 1, pp. 1-24
[7] Mouhti, I. A., *et al*., Characterization of CsI(Tl) and LYSO(Ce) Scintillator Detectors by Measurements and Monte Carlo Simulations, *Appl. Radiat. Isot., 154* (2019), 12, 108878
[8] Mitra, P. M., *et al*., Optimization of Parameters for a CsI(Tl) Scintillator Detector Using GEANT4-Based Monte Carlo Simulation Including Optical Photon Transport, *IEEE Trans. Nucl. Sci., 66* (2019), 7, pp. 1870-1878
[9] Khodaei., A., *et al.*, A Review of the Geant4 Simulation Platform for Applications Involving Optical-Based Sensing and Dosimetry, *Radiat. Phys. Chem., 212* (2023), 11, 111062

Received on April 8, 2024
Accepted on June 14, 2024

**Симин СЈАО, Синглунг ЛИ, Јанг ЉУ, Џипинг ЛУО,
Хунгчао ПАНГ, Ђенхуа ВУ, Сјаопенг ХУАНГ**

ПРЕНОСИВИ МЕРАЧ X/ -ЗРАЧЕЊА ЗАСНОВАН НА МРЕЖИ ИНТЕРНЕТА СТВАРИ ЗА МЕРЕЊЕ РАСПОДЕЛЕ ЗРАЧЕЊА У ЖИВОТНОЈ СРЕДИНИ

Детекција у реалном времену дозе X/ -зрачења има посебан значај у нуклеарним научним истраживањима. У овом раду, развили смо преносиви мерач X/ -зрака за масовно дистрибуирано праћење у реалном времену јачине еквивалента амбијенталне дозе у околној средини. Овај иновативни уређај користи силицијумски фотомултипликатор у комбинацији са CsI(Tl) сцинтилатором и може се повезати на мрежу Интернета ствари. Поред тога, олакшава широк спектар мерења јачине дозе модификујући фреквенцију dc-dc режима напајања типа импулсно-фреквентне модулације. Енергетски одзив анкетног мерача, који је побољшан кроз Geant4 симулације и дизајн са више компаратора, креће се од 48 keV до 1,3 MeV, обухватајући различите уобичајене апликације нивоа заштите. Ефикасно мери стопе дозе зрачења у распону су између 0,1 μSvh^{-1} и 100 mSvh^{-1} за ^{60}Co. Температурна компензација детектора постигнута је низом експеримената; мерач показује одступање од –25 % до +25 % на температурама између –40 °C и +40 °C.

Кључне речи: CsI(Tl) сцинтилатор, силицијумски фотомултипликатор, мерач X/γ-зрака, блутут, Интернет ствари